Inorganic Graphene Analogues

DOI: 10.1002/anie.201304337

Ultrathin Nanosheets of Vanadium Diselenide: A Metallic Two-Dimensional Material with Ferromagnetic Charge-Density-Wave Behavior**

Kun Xu, Pengzuo Chen, Xiuling Li, Changzheng Wu, Yuqiao Guo, Jiyin Zhao, Xiaojun Wu, and Yi Xie**

Over the past few years, graphene, which consists of a single layer of carbon atoms in a two-dimensional (2D) planar arranged as a honeycomb lattice structure, has attracted great attention owing to its unique and fascinating physical properties.[1–3] Meanwhile, inorganic 2D materials with graphene-like structure, especially those ultrathin nanosheets of transition metal dichalcogenide (TMD) with single or few atomic layers, have also been extensively studied owing to their special structures and rich electronic properties catering for intriguing applications such as energy storage and conversion, sensors,[4–6] and optoelectronic[7] and spinelectronic devices.[8,9] Representive TMD ultrathin nanosheets of TiS_2,[10] $TiSe_2$,[11] MoS_2,[12,13] $MoSe_2$,[14] WS_2,[15,16] WSe_2,[17,18] and VS_2[19,20] were gradually unraveled in recent years. However, it is still a major challenge to integrate exotic electronic charge and spin properties in the 2D TMD materials, which are intriguing possibilities for future-generation nanoelectronics.[21] Therefore, developing a new type of 2D TMD materials with exotic electronic charge and spin properties beyond current systems, is extremely urgent.

Vanadium diselenide (VSe_2), a typical layered TMD material, is made up of layers composing of metal V atoms sandwiched between two Se atom layers to give VSe_2 formula (CdI_2-type structure), and the Se-V-Se layers are further stacked by van der Waals interaction forming VSe_2 crystal form.[22] Furthermore, in the VSe_2 structure, the infinite V^{4+}-V^{4+} chains along a and b axis forms a V^{4+}-V^{4+} network structure in the *ab* plane, and there is a strong electron coupling interaction for all neighboring V^{4+}-V^{4+}, causing metallic character as well as the prototype charge-density-wave (CDW) behavior. Moreover, the $3d^1$ odd-electronic configuration of the V^{4+} ion also provides rich spin-related information. Recent theoretical investigations unraveled that the VSe_2 monolayer exhibit intrinsic magnetic behavior, and its magnetic moments and strength of magnetic coupling could even be tuned by isotropic strain.[23] Therefore, with synergic effects of $3d^1$ odd-electron configuration and their strong electron–electron correlations, VSe_2 ultrathin nanosheets would be a new type of 2D TMD that possessing exotic electronic charge and spin properties for future-generation electronics.

The theoretical calculations on of VSe_2 bulk and monolayers suggested that it would be feasible to achieve 2D VSe_2 sheets through an exfoliation process. As for bulk VSe_2, the in-plane electronic structure and electronic states along the *c* axis were revealed by the dispersions along the high-symmetry points Γ(k=(0,0,0)), M(k=(1/2, 0,0)), and K(k=(1/3,1/3,0)) on the Brillouin zone and dispersion along Γ(k=-(0,0,0) to A (k = (0,0,1/2)), as shown in Figure 1 c,d. The band structures of the in-plane Γ-M-K-Γ Brillouin symmetry point zone for bulk and monolayer VSe_2 are nearly identical, which

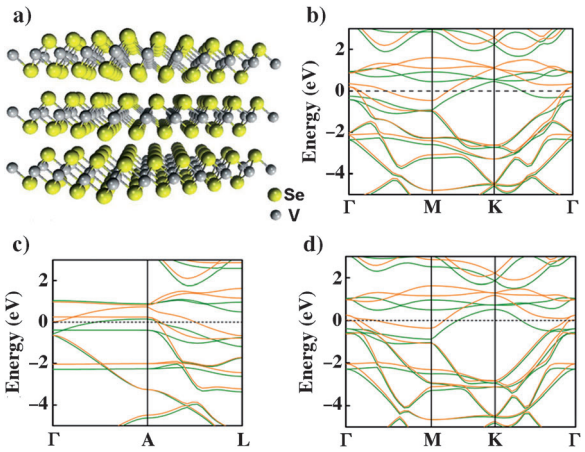

Figure 1. a) Side view of the atomic structure of a VSe_2 crystal. b) Band structure diagrams of VSe_2 monolayer; c) Band structure diagrams of bulk VSe_2 with symmetry zone segments of Γ-A-L; d) Band structure diagrams of bulk VSe_2 in-plane Γ-M-K-Γ symmetry points. Green = spin up, orange = spin down.

[*] K. Xu, P. Z. Chen, Prof. C. Z. Wu, Dr. Y. Q. Guo, Dr. J. Y. Zhao, Prof. X. J. Wu, Prof. Y. Xie
Hefei National Laboratory for Physical Sciences at Microscale and Collaborative Innovation Center of Chemistry for Energy Materials
University of Science & Technology of China
Hefei, Anhui 230026 (P.R. China)
E-mail: czwu@ustc.edu.cn
yxie@ustc.edu.cn
X. L. Li, Prof. X. J. Wu
CAS Key Laboratory of Materials for Energy Conversion and Department of Material Science and Engineering
University of Science & Technology of China
Hefei, Anhui 230026 (P.R. China)

[**] This work was financially supported by the National Basic Research Program of China (No. 2009CB939901), National Natural Science Foundation of China (No. 21222101, 11074229, 11132009, 11079004, J1030412), Chinese Academy of Science (XDB01020300), Program for New Century Excellent Talents in University and the Fundamental Research Funds for the Central Universities (No. WK2340000035 and WK2310000024).

Supporting information for this article is available on the WWW under http://dx.doi.org/10.1002/anie.201304337.

demonstrated that the interlayer interactions between layers are very weak (Figure 1 b,d). In Figure 1 c, the Γ-A segment of bulk VSe_2 (along the *c* axis) shows the flat lines or degenerate curves, giving evidence for weak electronic correlation along the *c* axis with no strong bonding force between each two neighboring Se-V-Se layers.[24] In this regard, weak interaction effect between each atomic layers along the *c* axis shows the capability of potential exfoliation of bulk VSe_2 into ultrathin nanosheets.

Despite of the theoretical feasibility, the technical realization of 2D VSe_2 ultrathin nanosheets with a graphene-like structure has not been realized so far. Herein, we highlighted the experimental realization of VSe_2 ultrathin nanosheets with 4–8 Se-V-Se atomic layers, as a new metallic inorganic 2D material, by liquid exfoliation of a bulk VSe_2 crystal in formamide solvent. In our case, bulk VSe_2 has been successfully synthesized in aqueous solution for the first time through a HCOOH co-reduction reaction route. This wet chemical pathway could be further extended as a general chemical strategy to prepare other metal selenides. As for the VSe_2 structure, the presence of V $3d^1$ odd electrons as well as the V-V atomic orbital overlapping enable it as a new metallic 2D material with unique electronic properties. The reduced dimensionality in the ultrathin nanosheets promotes the CDW transition temperature of VSe_2. To the best of our knowledge, VSe_2 is the first experimental case for quasi-2D materials having the features of both CDW behavior and room-temperature ferromagnetism (RTFM).

Employing HCOOH as a reducing agent has opened up a facile new approach to the preparation of bulk VSe_2 in aqueous solution. Scheme 1 a shows the formation mechanism of VSe_2 in aqueous solution. In this case, HCOOH was selected as reducing agent owing to the co-reduction processes from SeO_2 to H_2Se and from V^V to V^{IV}. Upon the coexistence of V^{IV} and H_2Se in aqueous solution, the formation of VSe_2 is inevitable. The whole process to form VSe_2 only involves a conventional hydrothermal method, thus avoiding the rigid high-temperature and time-consuming solid-state process and the use of complex equipment, thereby offering high operational convenience and short reaction time.[25] Furthermore, synthesis of VSe_2 in aqueous solution is a more sustainable reaction route, avoiding the employment of expensive organic solvents as well as the high toxic VCl_4 during whole process.[26]

Interestingly, the HCOOH-reduction reaction pathway in aqueous solution could be extended to prepare other metal selenides, such as SnSe, Ag_2Se, CdSe, NiSe, PbSe, and ZnSe. The formation processes of other metal selenides were all due to the HCOOH co-reduction of metal ions to lower-valence ions and SeO_2 to Se^{2-} (Scheme 1 b). For SnSe, the HCOOH could reduce SeO_2 and Sn^{4+} to H_2Se and Sn^{2+} in aqueous solution and then the SnSe precipitated out from the reaction system. On account of the weak reducing power of HCOOH, metal ions such as Ag^+, Cd^{2+}, Ni^{2+}, Pb^{2+}, and Zn^{2+} could not be reduced to elemental metal, and then these metal ions could directly combine H_2Se in aqueous solution to generate metal selenides. Thus aqueous-solution synthesis of various selenides has been successfully established based on the similar reaction mechanism. Other strong reducing agents,

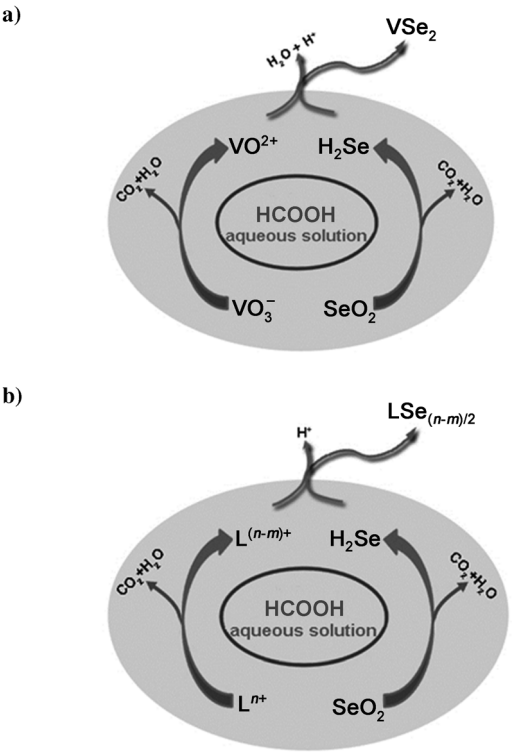

Scheme 1. Representation of the formation mechanism of a) VSe_2 and b) other metal selenides. L^{n+} represents Sn^{4+}, Ag^+, Cd^{2+}, Ni^{2+}, Pb^{2+}, Zn^{2+}, and so on. $0 \le m < n$.

such as hydrazine hydrate ($N_2H_4 \cdot H_2O$) and sodium borohydride ($NaBH_4$) have been successfully used for preparing selenides in aqueous solution.[27–29] However, the strong reducing ability greatly influenced valence states of metal ions, preventing them to be extended to be a general methods for preparing selenides in aqueous solution. In our case, the weak chemical reduction effect of formic acid (HCOOH) renders the opportunity to successfully establish a general reaction route. As a fact, a serial of metal selenides have been synthesized in the aqueous solution, including vanadium diselenide (VSe_2) which is known to be a hard-to-access TMD material. Our new synthetic strategy developed here paves a sustainable and economic way to the synthesis of selenides, compared with traditional methods that usually involves organic solvents as well as harsh reaction conditions.[25,30,31]

Synthesis of layered 1-T VSe_2 is a prerequisite for obtaining ultrathin nanosheets of VSe_2. As shown in Figure 2 b, all the diffraction peaks in X-ray diffraction (XRD) pattern of the as-synthesized bulk VSe_2 can be readily indexed to the hexagonal VSe_2 phase ($a = b = 3.3587$ Å, $c = 6.1075$ Å, $\alpha = \beta = 90°, \gamma = 120°$; JCPDS card No.89-1641). No other obvious impurities can be observed, revealing that the as-synthesized VSe_2 product was of high quality. Liquid exfoliation by surface energy matching has been shown to be an effective way to prepare 2D ultrathin nanosheets of layered compounds, including the transition-metal chalcogenides.[32] In our case, the typical layer-structured 1T-VSe_2 is also expected to be easily exfoliated into ultrathin nanosheets upon undergoing the liquid exfoliation process. We found that

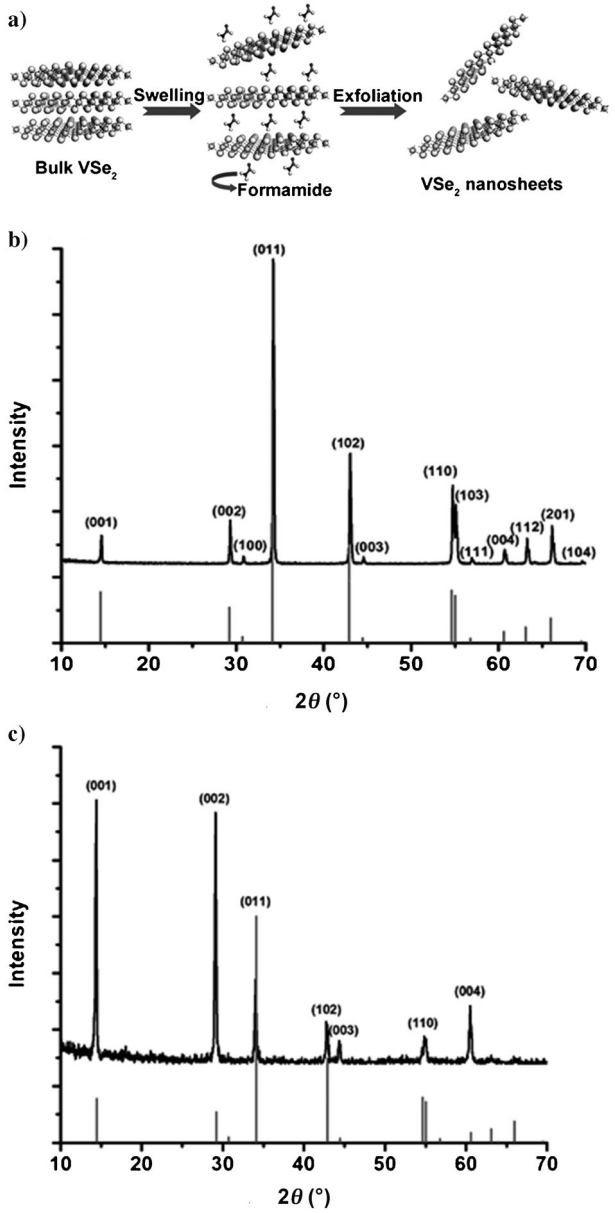

Figure 2. a) The liquid-exfoliation process from bulk VSe_2 to VSe_2 ultrathin nanosheets. b) XRD pattern of bulk VSe_2. c) XRD pattern of a thin film of VSe_2 ultrathin nanosheets. Data from JCPDS card no. 89-1641 is shown at the bottom of (b) and (c) for comparison.

the formamide could be established as the most efficient solvent to exfoliate bulk VSe_2 owing to their closer surface energies (Supporting Information, Section S4). As illustrated in Figure 2a, formamide molecules are initially intercalated into the layer space of the bulk VSe_2, resulting in a significantly expansion of interlayer spacing and then further weakening van der Waals interactions between the neighboring layers. Subsequently, VSe_2 ultrathin nanosheets were obtained by mechanical vibration. As performing the XRD characterization on an individual VSe_2 ultrathin nanosheet is infeasible, we fabricated a layer-by-layer assembled thin film by vacuum filtration methods. As expected, the relative intensity of peaks in XRD pattern of thin film is quite different from that of bulk VSe_2 sample (Figure 2b), in which the intensity of (*00l*) peaks present a distinctly enhanced value and other peaks are suppressed in the XRD pattern of VSe_2 thin film (Figure 2c). The XRD pattern exhibits the highly crystalline orientation along [001] axis for the ultrathin nanosheet thin films, indicating high quality of 2D VSe_2 nanosheet.

Microscopic characterizations were also carried out to further study phase and morphology of our VSe_2 ultrathin nanosheets. Transmission electron microscope (TEM) image of the VSe_2 nanosheets revealed that the as-obtained nanosheets are freestanding with an average diameter above 200 nm (Figure 3a). Notably, our observation of Tyndall

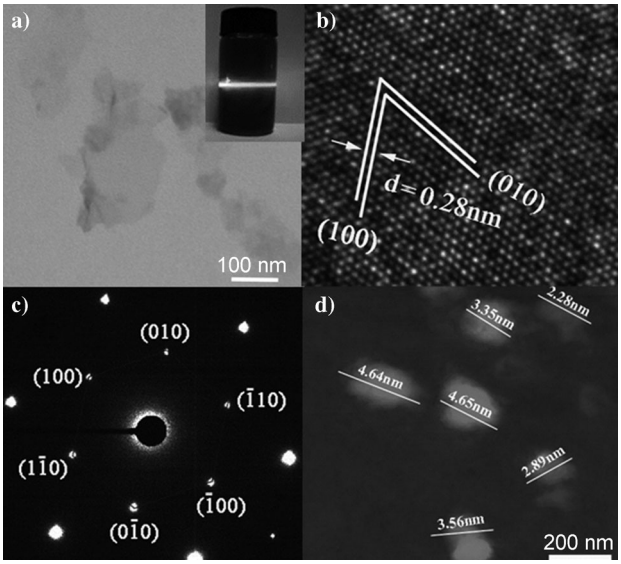

Figure 3. a) TEM image of an ultrathin VSe_2 nanosheet. Inset: Tyndall effect of the VSe_2 nanosheet solution. b) High-resolution TEM image of the VSe_2 ultrathin nanosheets. c) The corresponding SAED pattern. d) AFM image of the VSe_2 ultrathin nanosheets.

effect in the VSe_2 nanosheets solution provides strong evidence for the freestanding and homogeneous 2D ultrathin nanosheets. As shown in Figure 3b,c, HRTEM image and SAED were used to further reveal microstructural information, clearly demonstrating that the nanosheet is a hexagonal single crystal with [001] orientation. The thickness of the exfoliated nanosheets was evaluated from tapping mode in atomic force microscopy (AFM). The AFM images shown in Figure 3d reveals that the height of the exfoliated nanosheets were measured to be ranging from 2.28 nm to 4.65 nm, which means that the nanosheets are composed of about 4–8 Se-V-Se atomic layers (a single-layer VSe_2 slab along the [001] direction is 0.61 nm). These characterization results verified that the bulk 1T-VSe_2 have been successfully exfoliated into 2D ultrathin nanosheets with high crystallinity and high *c* axis orientation.

In the quasi-2D VSe_2 structure, the V^{4+}-V^{4+} strong electron correlation effect and the V^{4+} $3d^1$ odd electronic configuration endow it unique electrical and magnetic

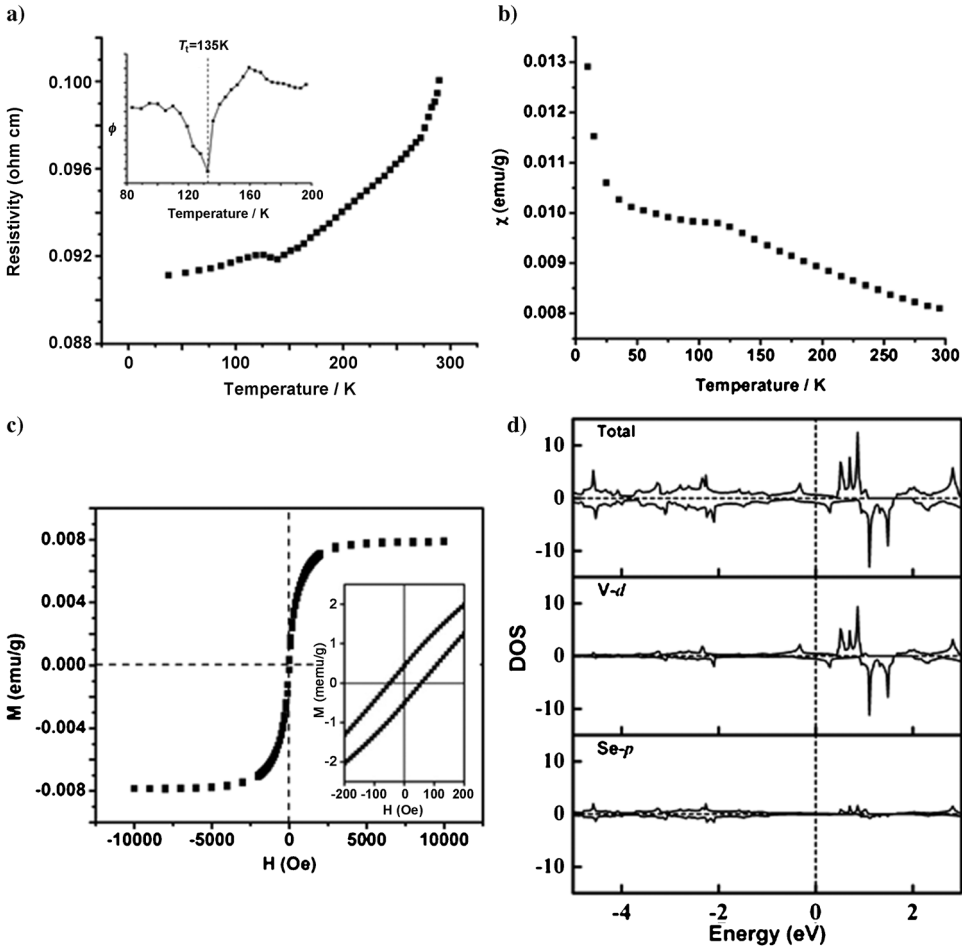

Figure 4. a) Temperature dependence of resistance. Inset: the differential resistivity versus temperature T in the temperature range 80–200 K. b) Temperature dependence of ZFC magnetization of the obtained ultrathin VSe_2 nanosheets. c) M–H curves of the obtained ultrathin VSe_2 nanosheets at 300 K. Inset: enlarged central section of (c). d) TDOS and PDOS of VSe_2 monolayer. The Fermi level is set at 0 eV.

properties. As shown in Figure 4a, the temperature dependence of resistivity of the obtained VSe_2 ultrathin nanosheets clearly shows a tendency of increasing electrical resistivity with the increasing temperature, showing the typical metallic behavior of our VSe_2 ultrathin nanosheets. The VSe_2 ultrathin nanosheets reached a relatively high electrical conductivity of $1\times10^3\,S\,m^{-1}$ at room temperature. Moreover, the temperature-dependent electrical resistivity curve also brings an abnormal resistivity bump around 135 K, which corresponds to the CDW transition of VSe_2 nanosheets. Also, CDW transition of the VSe_2 ultrathin nanosheets is observed by zero-field cooling (ZFC) magnetization as displayed in Figure 4b, showing an anomalous jump at the temperature around 135 K. Of note, the CDW transition temperature of the obtained bulk VSe_2 was around 107 K (Supporting Information, Figure S7), and the CDW transition temperature of 2D VSe_2 ultrathin nanosheets was regulated to higher temperature of 135 K owing to the dimensional reduction of 2D ultrathin structure.[11,33,34]

Figure 4c shows the magnetic field dependence of magnetization (M-H) at 300 K for as-prepared ultrathin nanosheets of VSe_2. The M-H curve exhibits a clear hysteresis loop which offers a solid evidence to demonstrate that the ultrathin nanosheets of VSe_2 is ferromagnetic at room temperature, while is not paramagnetic or superparamagnetic. From the M-H curve measured at 300 K, the saturation magnetization (M_s) value of VSe_2 ultrathin nanosheets can be extracted to be 0.008 emu g^{-1}. The coercivity of ultrathin nanosheets of VSe_2 is about 43 Oe which has also established by the enlarged M-H curve in the low-field region (Figure 4c, inset). Moreover, we have also performed a first-principles calculations based on density functional theory and confirmed the intrinsic ferromagnetism of the ultrathin nanosheets of VSe_2. A $2\times2\times1$ supercell of VSe_2 monolayer has been tested to clarify the magnetic coupling effect between different unit cells. The antiferromagnetic state is less stable than the ferromagnetic state, with an energy difference of about 0.1 eV. The total energy calculations clearly manifest that the RTFM state is the ground state to the monolayer VSe_2. The magnetic moment of vanadium atom per unit cell is about $0.693\mu_B$, while the magnetic moment of selenium atom is about $-0.046\mu_B$. The density of states (DOS) of the VSe_2 monolayer, shown in Figure 4d, demonstrates a significant asymmetry between the spin-up states and spin-down states. Furthermore, the detailed PDOS analysis of VSe_2 monolayer suggests that the V 3d orbitals gives primary contribution to the states near the Fermi level. Thus, both the experimental magnetic characterization and the theoretical analyses clearly verified the intrinsic RTFM of ultrathin nanosheets of VSe_2. To the best of our knowledge, VSe_2 ultrathin nanosheets is the first 2D TMD material with intrinsic RTFM and CDW state. Therefore, CDW VSe_2 ultrathin nanosheets could carry signs of electronic charge and spin in next-generation nanoelectronics.

In conclusion, we have successfully developed a new metallic inorganic 2D material, VSe_2 ultrathin nanosheets with 4–8 Se-V-Se atomic layers, by an effective liquid exfoliation method. Owing to the electron delocalization of the 2D vanadium lattice framework, VSe_2 ultrathin nanosheets possessed the intriguing high electrical condutivity ($1\times10^3\,S\,m^{-1}$) as a new inorganic 2D material with metallic behavior. And the VSe_2 ultrathin nanosheets with $3d^1$

electronic configuration is the first 2D TMD with intrinsic RTFM. The CDW transition temperature was also regulated to higher temperature of 135 K owing to the dimensional reduction to 2D ultrathin nanosheets. Realizing spin as well as exotic electronic charge behavior in a single 2D material is of great significance for constructing next generation 2D nanoelectronics especially for spintronic device; therefore, we anticipate that the VSe_2 ultrathin nanosheets would pave a new way to design next-generation spintronic devices and inspire more scientific interest in new types of 2D TMD materials with fascinating electronic properties.

Received: May 20, 2013
Revised: July 7, 2013
Published online: August 16, 2013

Keywords: charge density waves · metallic behavior · room temperature ferromagnetism · ultrathin nanosheets · vanadium selenide

[1] K. S. Novoselov, V. I. Falko, L. Colombo, P. R. Gellert, M. G. Schwab, K. Kim, *Nature* **2012**, *490*, 192 – 200.
[2] L. Vicarelli, M. S. Vitiello, D. Coquillat, A. Lombardo, A. C. Ferrari, W. Knap, M. Polini, V. Pellegrini, A. Tredicucci, *Nat. Mater.* **2012**, *11*, 865 – 871.
[3] H. Yan, X. Li, B. Chandra, G. Tulevski, Y. Wu, M. Freitag, W. Zhu, P. Avouris, F. Xia, *Nat. Nanotechnol.* **2012**, *7*, 330 – 334.
[4] C. Zhu, Z. Zeng, H. Li, F. Li, C. Fan, H. Zhang, *J. Am. Chem. Soc.* **2013**, *135*, 5998 – 6001.
[5] H. Li, Z. Yin, Q. He, H. Li, X. Huang, G. Lu, D. W. H. Fam, A. I. Y. Tok, Q. Zhang, H. Zhang, *Small* **2012**, *8*, 63 – 67.
[6] Q. He, Z. Zeng, Z. Yin, H. Li, S. Wu, X. Huang, H. Zhang, *Small* **2012**, *8*, 2994 – 2999.
[7] Z. Yin, H. Li, H. Li, L. Jiang, Y. Shi, Y. Sun, G. Lu, Q. Zhang, X. Chen, H. Zhang, *ACS Nano* **2012**, *6*, 74 – 80.
[8] X. Huang, Z. Zeng, H. Zhang, *Chem. Soc. Rev.* **2013**, *42*, 1934 – 1946.
[9] M. Chhowalla, H. S. Shin, G. Eda, L.-J. Li, K. P. Loh, H. Zhang, *Nat. Chem.* **2013**, *5*, 263 – 275.
[10] C. Lin, X. Zhu, J. Feng, C. Wu, S. Hu, J. Peng, Y. Guo, L. Peng, J. Zhao, J. Huang, J. Yang, Y. Xie, *J. Am. Chem. Soc.* **2013**, *135*, 5144 – 5151.
[11] P. Goli, J. Khan, D. Wickramaratne, R. K. Lake, A. A. Balandin, *Nano Lett.* **2012**, *12*, 5941 – 5945.
[12] Z. Zeng, Z. Yin, X. Huang, H. Li, Q. He, G. Lu, F. Boey, H. Zhang, *Angew. Chem.* **2011**, *123*, 11289 – 11293; *Angew. Chem. Int. Ed.* **2011**, *50*, 11093 – 11097.
[13] S. S. Chou, B. Kaehr, J. Kim, B. M. Foley, M. De, P. E. Hopkins, J. Huang, C. J. Brinker, V. P. Dravid, *Angew. Chem. Int. Ed.* **2013**, *52*, 4160 – 4164.
[14] S. Tongay, J. Zhou, C. Ataca, K. Lo, T. S. Matthews, J. Li, J. C. Grossman, J. Wu, *Nano Lett.* **2012**, *12*, 5576 – 5580.
[15] J.-w. Seo, Y.-w. Jun, S.-w. Park, H. Nah, T. Moon, B. Park, J.-G. Kim, Y. J. Kim, J. Cheon, *Angew. Chem. Int. Ed.* **2007**, *46*, 8828 – 8831.
[16] K.-G. Zhou, N.-N. Mao, H.-X. Wang, Y. Peng, H.-L. Zhang, *Angew. Chem.* **2011**, *123*, 11031 – 11034; *Angew. Chem. Int. Ed.* **2011**, *50*, 10839 – 10842.
[17] H. Fang, S. Chuang, T. C. Chang, K. Takei, T. Takahashi, A. Javey, *Nano Lett.* **2012**, *12*, 3788 – 3792.
[18] Z. Zeng, T. Sun, J. Zhu, X. Huang, Z. Yin, G. Lu, Z. Fan, Q. Yan, H. H. Hng, H. Zhang, *Angew. Chem.* **2012**, *124*, 9186 – 9190; *Angew. Chem. Int. Ed.* **2012**, *51*, 9052 – 9056.
[19] J. Feng, X. Sun, C. Wu, L. Peng, C. Lin, S. Hu, J. Yang, Y. Xie, *J. Am. Chem. Soc.* **2011**, *133*, 17832 – 17838.
[20] J. Feng, L. Peng, C. Wu, X. Sun, S. Hu, C. Lin, J. Dai, J. Yang, Y. Xie, *Adv. Mater.* **2012**, *24*, 1969 – 1974.
[21] Q. H. Wang, K. Kalantar-Zadeh, A. Kis, J. N. Coleman, M. S. Strano, *Nat. Nanotechnol.* **2012**, *7*, 699 – 712.
[22] M. Bayard, M. J. Sienko, *J. Solid State Chem.* **1976**, *19*, 325 – 329.
[23] Y. Ma, Y. Dai, M. Guo, C. Niu, Y. Zhu, B. Huang, *ACS Nano* **2012**, *6*, 1695 – 1701.
[24] H. Jiang, *J. Chem. Phys.* **2011**, *134*, 204705 – 204708.
[25] F. J. DiSalvo, J. V. Waszczak, *Phys. Rev. B* **1981**, *23*, 457 – 461.
[26] S. Jeong, D. Yoo, J.-t. Jang, M. Kim, J. Cheon, *J. Am. Chem. Soc.* **2012**, *134*, 18233 – 18236.
[27] Q. Peng, Y. Dong, Z. Deng, Y. Li, *Inorg. Chem.* **2002**, *41*, 5249 – 5254.
[28] H. Liu, H. Cui, F. Han, X. Li, J. Wang, R. I. Boughton, *Cryst. Growth Des.* **2005**, *5*, 1711 – 1714.
[29] H. Tong, Y.-J. Zhu, L.-X. Yang, L. Li, L. Zhang, *Angew. Chem.* **2006**, *118*, 7903 – 7906; *Angew. Chem. Int. Ed.* **2006**, *45*, 7739 – 7742.
[30] J. Yang, C. Xue, S.-H. Yu, J.-H. Zeng, Y.-T. Qian, *Angew. Chem.* **2002**, *114*, 4891 – 4894; *Angew. Chem. Int. Ed.* **2002**, *41*, 4697 – 4700.
[31] W. Wang, Y. Geng, P. Yan, F. Liu, Y. Xie, Y. Qian, *J. Am. Chem. Soc.* **1999**, *121*, 4062 – 4063.
[32] J. N. Coleman, M. Lotya, A. O'Neill, S. D. Bergin, P. J. King, U. Khan, K. Young, A. Gaucher, S. De, R. J. Smith, I. V. Shvets, S. K. Arora, G. Stanton, H.-Y. Kim, K. Lee, G. T. Kim, G. S. Duesberg, T. Hallam, J. J. Boland, J. J. Wang, J. F. Donegan, J. C. Grunlan, G. Moriarty, A. Shmeliov, R. J. Nicholls, J. M. Perkins, E. M. Grieveson, K. Theuwissen, D. W. McComb, P. D. Nellist, V. Nicolosi, *Science* **2011**, *331*, 568 – 571.
[33] Y. Ge, A. Y. Liu, *Phys. Rev. B* **2012**, *86*, 104101.
[34] M. Calandra, I. I. Mazin, F. Mauri, *Phys. Rev. B* **2009**, *80*, 241108.

